https://doi.org/10.3311/PPee.22669

Periodica Polytechnica Electrical Engineering and Computer Science, 68(4), pp. 367–380, 2024

Modeling and Study of Different Magnet Topologies in Rotor of Low Rating IPMSMs

Supriya Naik[1], Baidyanath Bag[1], Kandasamy Chandrasekaran[1*]

[1] Electrical Engineering Department, National Institute of Technology, G.E. Road, 492010 Raipur, Chhattisgarh, India
[*] Corresponding author, e-mail: kchandrasekaran.ee@nitrr.ac.in

Received: 27 May 2023, Accepted: 31 May 2024, Published online: 16 July 2024

Abstract

A study and performance analysis of magnet positions in different topology on the surface of rotor in permanent magnet synchronous motors (PMSMs) based on finite element method is observed here. A 3-phase interior PMSM is numerically simulated with ANSYS Maxwell 2018.1. Differently positioned permanent magnets improve the performance of PMSMs. Apart from handling nonlinear equations, FEM is used for simulation. ANSYS is used to analyze PMSM performance under variable conditions. This proposal examines a three-phase, 0.55 kW PMSM at 220 V, 50 Hz. Here rotor topologies of five types, namely, (i) spoke/tangential, (ii) saturable bridge / u-shape, (iii) V-shape, (iv) radial, and (v) segmented bridge permanent magnet rotor are taken for observation. The motive of this study is to analyze the performance of PMSMs in different rotor designs with different magnet positions. All topologies have been modeled and simulated with ANSYS. Each topology is compared in terms of electromagnetic and mechanical parameters. The 2D model is used to model the distribution of magnetic fields and the performance of operating parameters under transient and steady-state conditions. Magnetic flux, and efficiency are heavily influenced by the rotor shape with the volume of magnet. A study of radial force distribution and mechanical stress across rotor surface is also discussed. Motor performance is affected by the design of PMs.

Keywords

2D model, electromagnetic, mechanical parameters, demagnetization, finite element method (FEM), rotor topologies, permanent magnet synchronous motor (PMSM)

1 Introduction

A pillar of industrial application, induction motors (IMs) are considered to be the most widely used, but permanent magnet synchronous machines (PMSMs) are get into prominence, which have controlled over all kinds of markets, including industry, electric vehicles and hybrid electric vehicles, aircraft, and so on. In comparison to other traction motor technologies, its high efficiency, high value of power density, extended flux weakening region, and rugged construction all contribute to its high performance [1]. It was shown that PMSM has an extremely crucial role in the development of aircraft motors [2]. The cooling system of an IM is less robust than that of a PMSM, but its design is robust in comparison. As a result of the excitation windings in induction motors, maintenance is more complex and more power is required. Due to that, the motor is more complex to operate. Additionally, synchronous reluctance motors (SRMs) are the most widely used motor, because they are able to operate under harsh conditions and are fault-tolerant. But, it has low power factor and high acoustic noise. With advanced design, like magnetic gears, PMSM overcomes the limitations of IM and SRM for traction applications [3, 4]. Motor size and cost can be reduced by replacing excitation windings with permanent magnets (PMs). PMSM's high performance at low cost makes it an ideal choice for electric vehicle applications [5]. Further, PMSM has high value power factor and power density in low-rated applications compared to IM. In addition to IM, the DC motor was also replaced. PMSMs have greater heat transfer capacity, longer lifespan, and less audible noise than DC motors [6]. The motor was made simpler in terms of operation and design. Two kinds of PMSM exist:

1. surface mounted PM (SPM) and
2. interior PM (IPM).

A limitation of the earlier model is the inability to produce torque [7]. Most EVs use interior PM because of its

Cite this article as: Naik, S., Bag, B., Chandrasekaran, K. "Modeling and Study of Different Magnet Topologies in Rotor of Low Rating IPMSMs", Periodica Polytechnica Electrical Engineering and Computer Science, 68(4), pp. 367–380, 2024. https://doi.org/10.3311/PPee.22669

higher efficiency and variable speed [8]. SPM and IPM are compared in [9] in relation to dual rotor axial flux. Interior permanent magnet machines (IPMSMs) are required in hybrid electric vehicles for traction applications because they must have a higher power density with higher torque density, and a wide constant power speed range (CPSR) that is efficient, among other things [10]. A comparison between SPM and IPM rotors is made in [11]. SPM rotors run at higher speeds because of higher mechanical strength factor than IPM. In the other side, IPM mitigates the flux weakening ability of SPM motors with their relatively large physical airgap length. So, researcher has been focused on IPM. The CPSR is heavily influenced by rotor design of IPMSMs. The numerical analysis of these properties is carried out using a variety of techniques. In order to understand composite domain structure, numerical methods have been extensively employed. FEM is one of these techniques, and is capable of accurately calculating 2D/3D problems with complicated geometries. In [12], FEM has chosen for solving a standard benchmark problem. The ANSYS Maxwell software is employed to observe the operation of a three phase PMSM in [13]. This platform can analyze all conditions in direct way, such as transient states, steady states, magnetostatic conditions, etc. A 2-D FE analysis (FEA) was used in addition to a 3-D FEA to reduce computation time. 2D FEM is therefore termed as vital tool in the primary analysis of electrical machines. A FEM analysis requires detail about the geometry, the type of use, and the boundary conditions [14]. Power factor, phase current, output torque, and efficiency are some of the factors that effect on due to rotor design variables. Advances in PM based electric machines, which utilize many optimization techniques and modification of stator mechanical parameters, have been discussed in the literature [15, 16]. A major focus of this study is to understand how the PM's position on the rotor affects the output parameters of IPM. There are several key parameters in the stator, including the slot fill factor, lamination factor, slot width, and tooth height. To improve power efficiency, the maximum slot filling factor for high frequency applications is 0.75 [17]. The same is considered in this study for theoretical analysis. A low frequency application requires a lamination factor of 0.9. This study considers the same, which decreases eddy currents. Hence, the PM cannot affect the air-gap magneto-motive force distribution under the same projection when placed within the rotor core, so it can be moved to get different motors based on the PM position within the core part of rotor [18]. Rotor designs of different types have been discussed in [19]. The alignment of PM on the surface of the rotor results different rotor designs. There is a limitation to this rotor design analysis and it is not applicable to all parameters of all rotor topologies. A permanent magnet in a rotor and teeth on a stator must be aligned magnetically when the electromagnetic torque (T_{em}) is to be generated. Ripple in T_{em} increases when magnetic flux distribution is non-sinusoidal, when it is saturated, when slots are incorrectly selected, etc. These damaging effects will also decrease start-up and stability of the motor. Due to their use in electric vehicles, which contain many high/low level voltage electrical components, IPM motors need to be highly carefully selected for their electromagnetic environment [20]. Thus, all machine topologies must be understood with regard to electromagnetic compatibility. In [21], SPM and IPM types having different magnet position are compared. In [22, 23], V-shaped IPMSM is discussed due to its high speed quality, its modified topologies and projected a comparative study with extracted three topologies. In [24], five topologies are compared which consists of spoke, U-shape, V-shape, straight shape rotors but V-shaped and spoke-shaped IPMSM are more focused due to its high torque and efficiency factor.

This paper presents a comparative study of five common IPM rotor topologies:

1. spoke/tangential,
2. saturable bridge/u-shape,
3. V-shape,
4. radial, and
5. segmented bridge permanent magnet (PM) based on their designing and performance.

All literature described here are focused on single with multi-layer comparison. Before considering multi-layer, it is necessary to know the basic characteristics of all kinds of single layer designs. Selection of topologies are based on considered literatures and previous studies in [4, 5, 19, 21–24]. Basic design includes spokes and radials, and the rest three topologies modify them. Here, only single layer topologies are considered for comparative study. Moreover, restricted basic design is discussed with examples in the literature. It is also possible to implement precise magnetic circuits in IPMs using multilayered magnet configurations or multi-segmented magnet configurations. Before modifying a more basic design under transient and steady state states, it is important to observe its characteristics. Manufacturers will be able to reduce costs

and timeliness by doing this. Electromechanical, electromagnetic, and PM demagnetization capabilities are taken for the performance analysis of these basic rotor designs. It is clear from these parameters that they are used for a variety of purposes. According to the following structure, this article is organized. PMSM modeling in ANSYS MAXWELL is covered in Section 2, specifically IPMSM using mathematical expressions for electromagnetic analysis. Section 3 discusses the five topologies of IPM motors as well as their designing. A comparison of the electromagnetic and electromechanical properties of all five topologies is presented in Section 4 to confirm their merits and demerits. Results and conclusions of the numerical experiments are presented in Section 5.

2 Modeling of IPMSM using FEM

As shown in Fig. 1, a flowchart is presented that illustrates the entire process of designing and analyzing PMSM machines. Several steps were followed to design the IPMSM machine, including choosing the properties of required materials, resizing the geometry of design parameters in the stator slots and rotor surface sections such as width of slot (W_{s1}), height of slot (H_{s1}), opening base width (B_{s0}), stator teeth slant height (H_{s2}), and positions of PM relative to the shaft band. The position of magnet with respect to shaft and stator parts and in rotor region are resulting variety of IPMSMs types. Including that, stator winding property and its insulation details, poles details, design of shaft, number of slots with motor rating are involved as a fixed parameters a in generation of motor model. If these settings are incorrect then the motor model is impossible to validate itself for FEM analysis. So, value of each design parameter is important. Maxwell's partial differential equations have been discussed in [1], and magnetic field distribution over the motor model is determined by using numerical methods in the processing section. The equilibrium equations are calculated by integrating the phase currents of the rotor with the flux density and all other electromagnetic performance parameters of motor. It is necessary to include the equilibrium equation of each component in order to make equations for the whole model, which ensure continuity at each node. IPMSM in ANSYS Maxwell is analyzed using Maxwell's equations for magnetostatic and magnetotransient analysis. The electromagnetic torque expressed in Eq. (1) can be determined by using the factors such as number of pole pairs of stator and rotor parts (p), PM's flux density (Ψ_{PM}) and quantities like current and inductances along q- and d-axis as given in Eq. (1) [3]:

$$T = \frac{3}{2} p\left(\Psi_{PM} i_q + \left(L_q - L_d\right) i_d i_q\right). \tag{1}$$

Basic three phases a, b, and c quantities are determined the inductance (L_d and L_q) and current (i_d and i_q) along q- and d-axis.

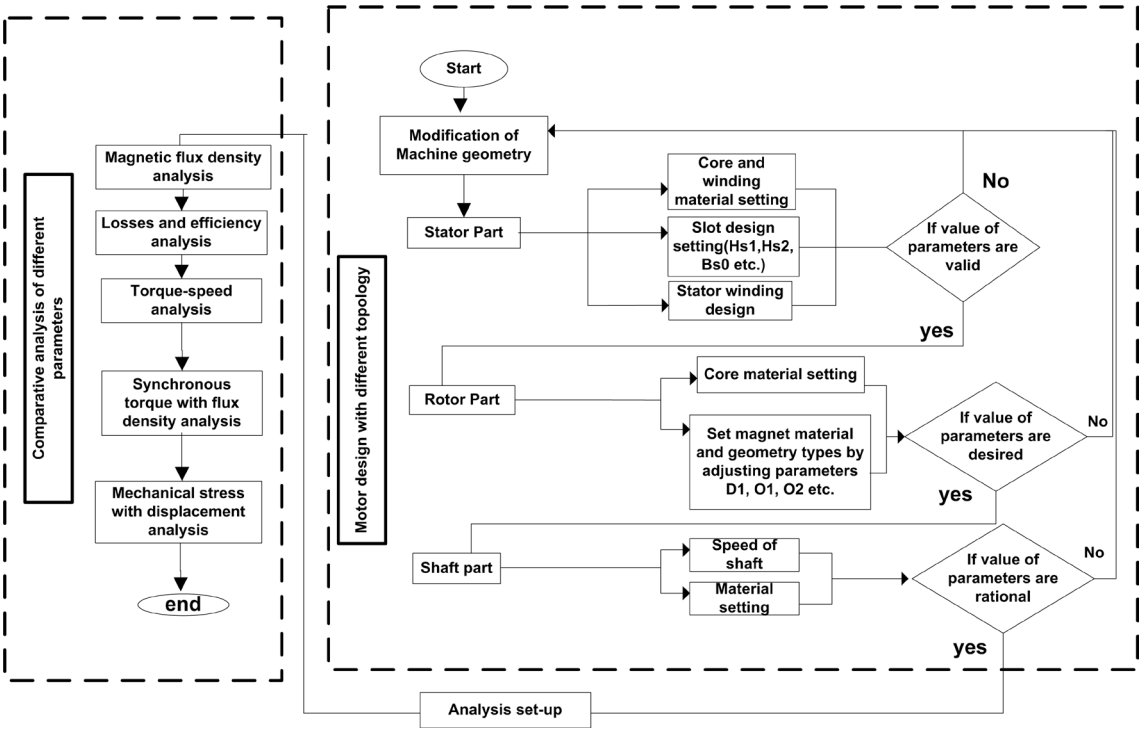

Fig. 1 Methodology of IPMSM designs and comparative study of different parameters

3 Different topologies of IPMSM rotor

The design parameters for the motor are restricted within the limits to include 24 slots for the stator and 4 poles for the rotor. A total of five topologies were designed for PM rotors of IPM motors, as illustrated in Fig. 2 (a) to (e). In Fig. 2, it can be seen that magnet topologies differ based on magnet block numbers and magnetization directions for each pole. Fig. 2 (a) and (d) illustrate how these two basic topologies are used in other designs. Fig. 2 (b), (c), and (e) show a multi-segment motor with high fabrication complexity and optimal magnet segmentation in order to increase cogging torque and average air gap flux density. Various ancillary geometric parameters, including thickness, and width, are examined for each topology in order to determine its location, the flux barrier bridges, and their distance from it. D1 determines the radius of expansion of the magnet in the rotor region, which is measured from the circumference of the rotor. In all PM topologies, O2 defines as the vertical distance between midpoints of magnetic poles and circumference of motor shaft. Except spoke-shape, rest topologies of motors use Rib to represent the closest distance between two adjacent poles. Rib is a measure of how far the magnet pole sits from the shaft of a motor in spoke-type motors. With *u*, *v*, and segmented topologies, O1 is defined as the bridge length between each pole. A spoke magnet topology uses B1 as the diameter from which the magnet expands. Meanwhile, a radial magnet topology uses the same parameter to explain the width of the flux barrier bridges. All topologies considered in this study have a 65 mm diameter shaft (D-shaft). Geometric features are being included in more and more circuit designs, which is resulting in a more complex designing process. Hence, the preliminary design stage predicts each quantity's maximum and minimum permissible values. Following that, each topology is analyzed using a 2D parametric finite element (FE) model. An analysis of the machine's performance based on the sensitivity and post-processing shows that the above parameters have an impact on its overall performance. Designed to reach a variety of constant powers, all five topologies utilize the stator having same single-layer distributed-winding. A wide range of operating speeds at constant power is required to achieve the performance necessary for hybrid electric vehicles, which is why all of the topologies represented in Fig. 2 (a) to (e) have been considered suitable candidates for operating at a wide operating speed.

The five machine designs were limited by the same nominal voltage and current. Motor rotors are designed to have an outer diameter of 74 mm and an air gap of 1 mm. The lower price of ferrite permanent magnets has led to the appearance of these magnets on rotor surfaces in many PMSMs. Ferrite PM, however, has been found to have a lower energy product, leading to increased dimensions [14]. In this design, neodymium–iron–boron (NdFeB35) PMs exhibit high remanences and have an increased coercive force in comparison with conventional permanent magnets [25].

Iron-based materials with good magnetic field capturing capabilities are selected for the stator and rotor designs. The coil size and wire gauge of the coil in a stator should be chosen properly to achieve 75% of the fill factor. IPM motor stators have an outer diameter of 120 mm. A design iteration

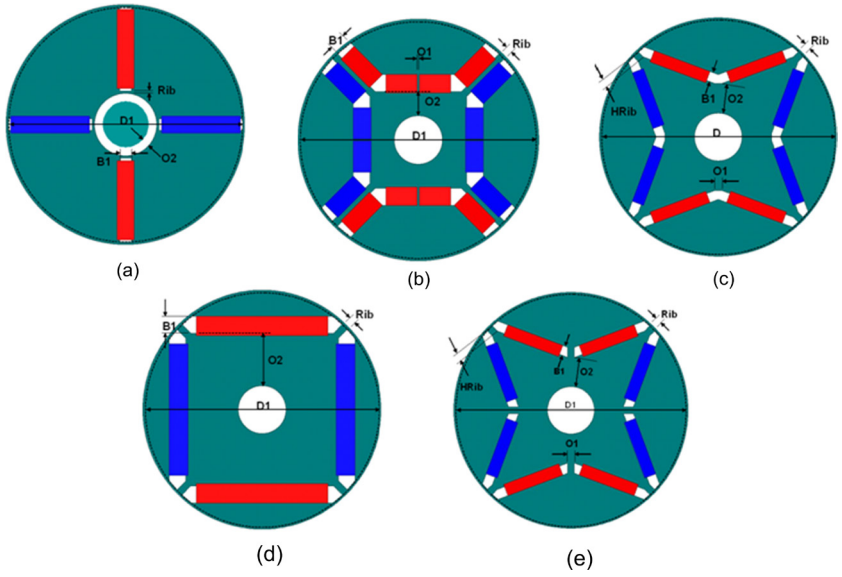

Fig. 2 Topologies of rotor of IPMSM; (a) spoke shape/tangential shape; (b) saturable bridge/ U-shape; (c) V-shape; (d) radial; and (e) segmented bridge

of machines is determined based on their overall performance, including mechanical and electromagnetic performance. This study examines underrated speed in terms of output torque, torque ripple, demagnetization ratio, cu-loss, eddy current loss, efficiency, and magnetic flux density. Simulations and analyses are used to estimate designs, which are refined and adjusted continually. A comparison of torque and speed characteristics has been conducted according to the design specifications, in order to confirm that each motor operates within its intended speed range. A comparison is also made between all five topologies based on flux linkage, flux density of airgap, and inductance.

4 Performance comparison of five IPMSM topologies

2-D FE models are utilized to analyze the performance of all five IPMSM topologies. In Table 1 [26], the stator design specification for the IPM motor is shown. For all topologies in the study, the stator design specification is used.

The stator is designed with distributed windings to produce a sinusoidal back electromotive force (BEMF). Due to the symmetry of the model, one fourth section of each motor is considered for comparison. In this study, all calculations are conducted at a temperature of 75 °C. The electromagnetic parameters of motors are measured using static FEA at operating temperatures and excitation with a d-q current. The first step in the analysis is to conduct a statistical comparison of parameters, followed by an analysis of each parameter separately. For traction operations, the static torque determines the required torque [27].

During rotor design, the volume of PM utilized in the rotor greatly influences the airgap flux density. PM rotor magnet thickness is closely related to air-gap flux density and rotor yoke flux density. It is the magnet's volume that defines its magnetic force. According to Fig. 3, the airgap flux density escalates with magnet width.

Table 1 Design parameters of the stator of 0.55 kW IPM motor [26]

Parameters	Value
Rated output power	550 W
Rated output torque	3.01 Nm
Line voltage rating	220 V
Resistance of stator	2.16 Ω
Synchronous speed	1500 rpm
Operating frequency	50 Hz
Phase current (in rms)	1.6 A
Peak phase current	2.4 A
Relative permeability of NdFeB35	1.099
Width of PM	3.5 mm

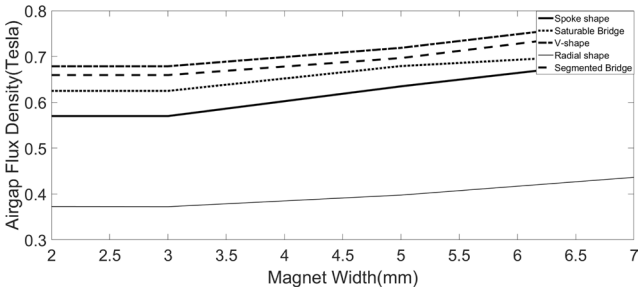

Fig. 3 Air gap flux density deviations with respected to magnet width of considered rotor topologies

Assume a slot-less magnetic field under air gap conditions. The V-shaped IPMSM has a higher flux density than other designs, as can be seen in Fig. 3. As a function of the magnet's width, the value of the air gap flux density increases. Depending on the inner diameter of the rotor, the magnet width varies. A range of 2 to 7 mm was considered in this study. Contour plots of the magnetic flux lines and it's density for each of the five topologies is presented in Table 2. All five topologies consider the magnet thickness to be the same. Among five models designed for low rating machines under no load conditions, the magnetic flux density does not differ significantly among the five topologies. Due to the reciprocity of stator and rotor magnetic fields, maximum magnetic flux density generates between the stator teeth during full load. When a spoke shape magnet rotor has a large number of flux lines, the magnetic flux density is highest there. There are also fewer flux lines attracting to magnetic shafts due to the presence of magnetic shaft. The rotor shaft area benefits from this factor from increased magnetic flux density. The magnetic shaft has improved the performance of the machine overall [28]. The maximum flux density is experienced by both end edges of the saturable bridge magnet. In the middle area of single poles, the flux density is reduced by saturable bridges with small flux barriers in the lower region. Since V-shaped rotors have the least amount of leakage flux, they provide the highest flux density of radial and spoke rotors. There is less flux barrier volume in V-shaped magnets. Shaft leakage flux occurs in spoke structures, whereas rotor leakage flux occurs in radial structures. Furthermore, magnetic flux is repulsive here with a single segment of PM. This will result in a lower flux density. The region of dense flux lines is the region in which all types of IPMSMs have the maximum flux density. According to Table 2, segmented bridges have the highest magnetic flux density compared to all other rotor topologies.

Table 2 Under no-load condition comparisons of magnetic flux density and flux lines

Rotor of topology	Magnetic flux density (Tesla)	Magnetic flux lines (A/m)
Spoke shape	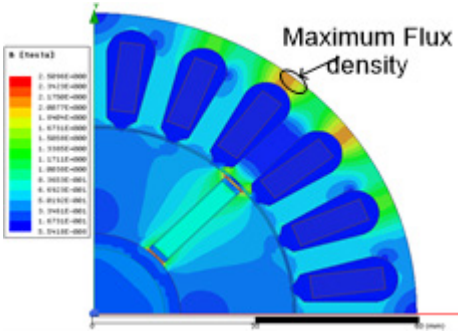	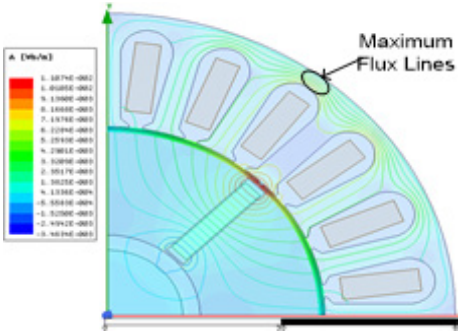
Saturable bridge	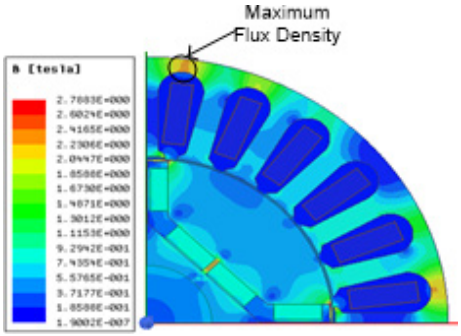	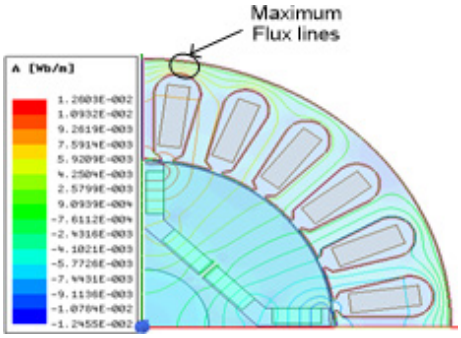
V-shape	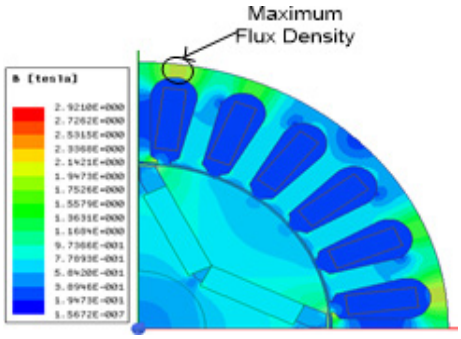	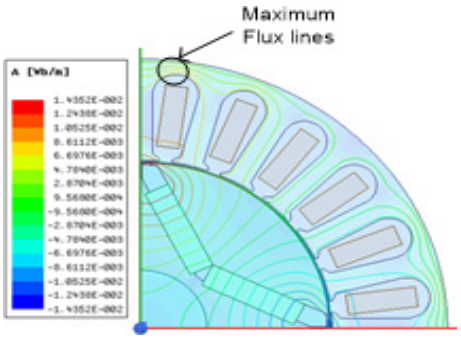
Radial shape	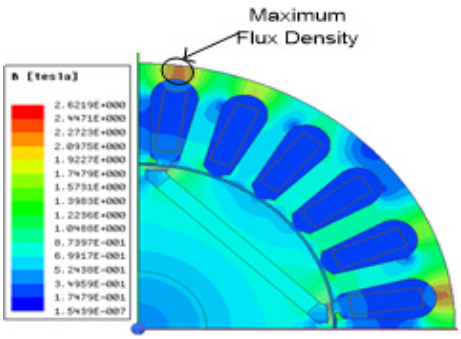	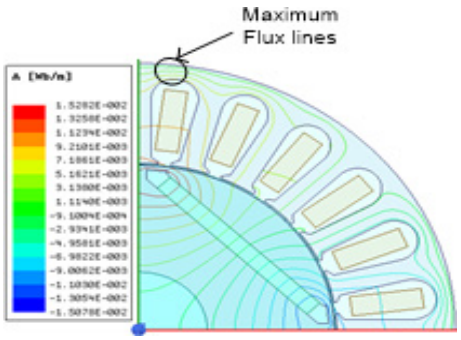
Segmented bridge	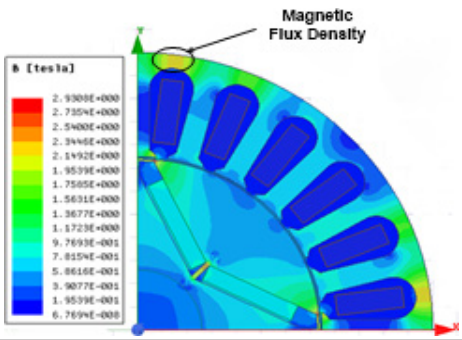	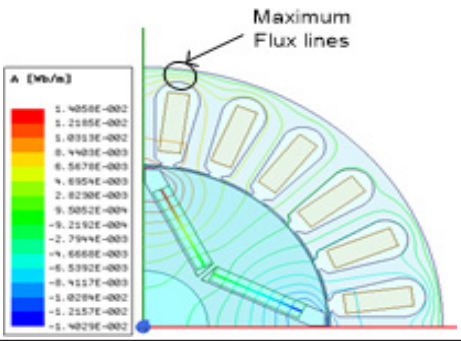

A SPM motor's inductance tends to be low, and the inductances of both axes are equal, which means it does not provide reluctance torque like an IPM motor. Working with an IPM motor involves large inductances in the d-axis, as well as the *q*-axis and on the *d*-axis. SPM machines are limited in terms of constant power speed range. There is a strong influence of inductances in the *d*-*q* axis on the behavior of PMSM. In addition, L_q is greater than L_d, and they are highly correlated to i_d and i_q. The torque of the motor is a good indicator of the motor's efficiency. There is only a slight difference between L_q and L_d for spoke shape rotors. In order to improve performance with power factor, their calculations are critical in terms of accessing torque and field attenuation powers [29].

An analysis of IPMSM parameters which involved inductance along the d- and q-axes under transient conditions is described in Table 3. According to Table 3, the spoke-shaped magnet has the highest d-axis inductance. The magnet rotor shaft and air gap end also leak flux, resulting in lower flux linkage. Thus, it is better suited for applications with wide speeds. The flux linkage of a radial shape rotor is the lowest, similar to that of a spoke type. There is a flux leak in the rotor in this case, as previously mentioned. All types of rotors have more flux linkage than saturable bridge shaped magnets. In the rotor part, there is less flux barrier due to less flux barrier region. Saliency ratio is used to calculate the torque capacity of a motor related to its power factor [30]. This is calculated as L_q / L_d. CPSR, a vital parameter of traction applications, is also enhanced by it. Machine flux weakening capacity is greatly affected by it. Saturable bridge and segmented magnet rotors have good saliency ratio as compared to the other three topologies, as shown in Table 3.

4.1 Losses and efficiency

The lamination cutting and punching process, the manufacturing process, the welding process, and stacking are played a significant role in iron loss. It is explored in this paper how these manufacturing processes impact each component of iron loss, including magnetization under saturation and coercive field strength. The five optimized IPMSM motors are compared in Fig. 4 under transient condition in terms of core loss and eddy current loss. In terms of core loss and eddy current loss, radial motors have the highest values. As a result of ferromagnetic material M36 being used for the manufacturing of the cores of the rotors and stators, these losses are obtained in low power applications. Designed machines are considered to have a zero lamination factor (i.e., without lamination of ferromagnetic material).

A significant difference between eddy current loss and hysteresis loss can be analyzed. Hence, eddy current losses and core losses are considered when comparing results. According to Fig. 4, core loss and eddy current losses are greater in motors with radial shapes. Core loss is 40.5%, 42.87% higher, eddy current loss is 55.09%, 58.66% higher than segmented and spoke rotors, respectively. Because of the less amount of magnet interaction between the rotor and stator tooth, there is less loss from eddy currents.

In this study, all topologies are affected by losses in terms of efficiency. As illustrated in Fig. 5, each rotor topology produces the same overall efficiency. With 86.6355% efficiency, spoke shape has a higher efficiency than other rotor topologies, due to the proportional relationship between efficiency and losses in the motor. Motors are considered in steady state here. As a result of this state, spoke shapes produce maximum torque output and have maximum airgap flux density average. Additionally, slot effect isn't taken into account when calculating efficiency.

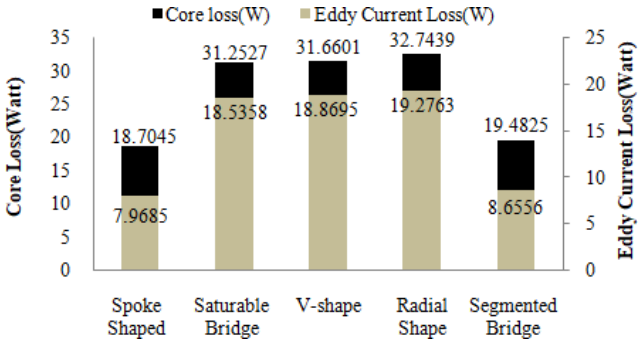

Fig. 4 Comparison of core and eddy current loss

Table 3 Comparison of motors parameters in the IPM motor designs

Rotor of topology	L_q	L_d	Saliency ratio of rotor	Flux linkage	Magnet weight
Spoke shape	11.1721 mH	19.2916 mH	0.5791	0.3201 Wb	0.1212 kg
Saturable bridge	16.7925 mH	13.5611 mH	1.2573	0.3283 Wb	0.2693 kg
V-shape	14.7743 mH	13.4591 mH	1.0977	0.3215 Wb	0.2693 kg
Radial shape	14.9057 mH	14.4326 mH	1.0327	0.3193 Wb	0.2693 kg
Segmented bridge	16.8859 mH	13.5554 mH	1.2456	0.3291 Wb	0.2693 kg

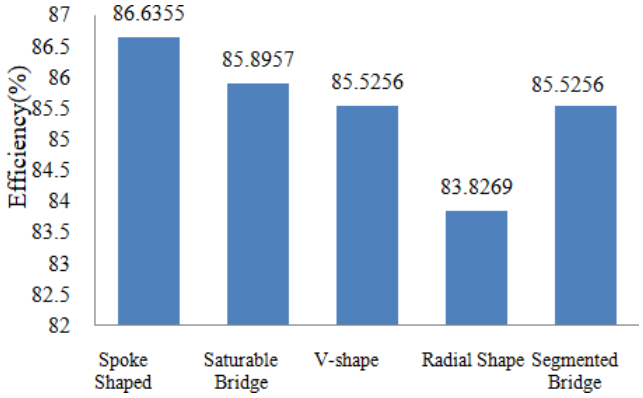

Fig. 5 Efficiency comparison of different rotor topology

4.2 Characteristics of starting and running state

Under rated condition, motor's performance characteristics have a higher value. The torque of each motor under rated conditions is illustrated in Fig. 6. In this graph, the spoke shape is more torque-intensive than the other shapes. It has high efficiency as well. Validating the PMSM design process requires a stable and dynamic model as well as simulation of the machine. Additionally, it eliminates unintended design errors that can occur in the construction and testing of machine prototypes [15]. In order to verify PMSM's starting and running torque for electric vehicles, it must be tested. At the beginning of Section 4, it is discussed as ripple torque. According to Fig. 6, all rotor designs under transient conditions achieve their maximum running torque. As shown in Fig. 6, there is nearly equal torque for the saturable bridge, V-shaped, and segmented bridge rotor designs. The spoke-shaped rotor had the minimum running torque, measuring 16.2522 Nm for all types of motor under study. As mentioned above, it has a lower value magnetic flux density as well. Under magnetic field analysis, spoke shape lacks a flux-intensify region.

When it comes to torque angle, the V-shaped rotor topology has the highest running torque. When the electrical

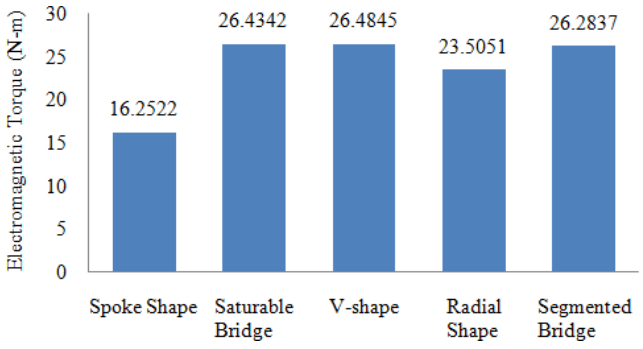

Fig. 6 Maximum electromagnetic torque (T_{em}) comparison under running conditions

torque angle is 80°–110° of steady-state, there is a running torque around this angle. Furthermore, as part of the design process for all types of rotor machines, torque is also simulated directly under transient conditions under the ANSYS Platform. The current study considers voltage source windings with armature resistances of 2.6573 Ω. Fig. 7 shows a comparison and plot of the results. In comparison with all other rotor shapes, the radial one has the highest starting torque.

When the rotor is not loaded, it has a nearly equal starting torque due to the presence of a saturable bridge and a V-shaped permanent magnet. It takes 20–25 m for the motor to synchronize from the start time. There is an atmospheric magnetic field that interlinks to stator armature reaction for producing electromagnetic torque. Because of the non-symmetric magnetic circuit of the *d*- and *q*-axes, the 2nd harmonic component is reluctance torque. It has already been explained why IPMs have a higher saliency ratio. IPM's power density and overloading ability are highly affected by reluctance torque. Reluctance torque opposes magnet torque, which is always negative. Depending on both magnetic and reluctance torque components, electromagnetic torque increases with current excitation angle.

The electromagnetic torque of an accelerating motor is always less than the magnetic torque of the same motor when the motor is running. Magnetic torque and reluctance torque are both defined by electromagnetic torque in Fig. 7. Table 4 illustrates the separation of electromagnetic torque. This segregation takes into account the average torque values.

Mechanical loading condition is used to analyze electromagnetic torque. It is shown in Fig. 8 that torques of all five topologies are considered for the analysis at 3.5 Nm load torque with a speed of 1500 rpm and rotation angle of 30° at starting. The torque angle and driving torque increase in mechanical transient conditions as the speed decreases. There is a reduction of ripple in the electromagnetic torque (T_{em}) due to the load torque (T_l). The saturable

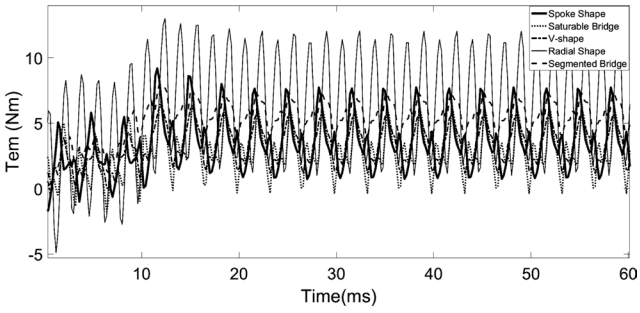

Fig. 7 Electromagnetic torque comparison under starting conditions

Table 4 Electromagnetic torque details in segregation

Rotor topology	Electromagnetic torque	Magnetic torque	Reluctance torque
Spoke shape	3.6977 Nm	−0.3953 Nm	4.0929 Nm
Saturable bridge	2.7551 Nm	−35.6004 Nm	38.3555 Nm
V-shape	4.3341 Nm	−0.1110 Nm	4.4450 Nm
Radial shape	6.5906 Nm	7.6920 Nm	−1.1074 Nm
Segmented bridge	5.6303 Nm	−8.2351 Nm	13.8658 Nm

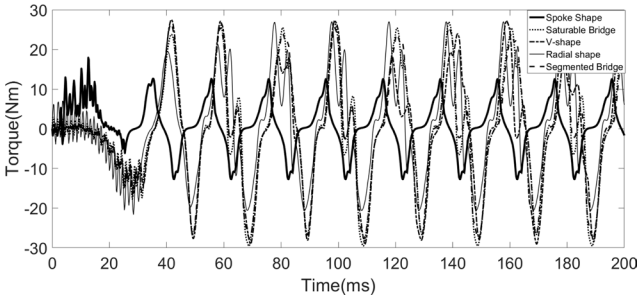

Fig. 8 Effect of load torque on electromagnetic torque

bridge has a smaller T_{em} characteristic than the other topologies. In this observation, the V-shape, radial, and segmented bridge has better characteristics.

4.3 Analysis of radial force

For all types of machines, radial forces are considered for estimating vibrations and analyzing acoustic noise. Analyzing the magnetic flux density vector $\boldsymbol{B}$, obtained from FEA, is a typical method of examining radial forces ($\boldsymbol{F}_r$). According to [11], $\boldsymbol{F}_r$ can generally be expressed by Eq. (2):

$$\boldsymbol{F}_r = \left(\frac{1}{2\mu 0}\right)\left(\boldsymbol{B}_r^2 - \boldsymbol{B}_t^2\right), \tag{2}$$

where radial force density represented by $\boldsymbol{F}_r$, radial component of magnetic flux density is denoted by $\boldsymbol{B}_r$, and for tangential component of magnetic flux density $\boldsymbol{B}_r$ is used. Magnetic flux density vectors have radial and tangential components that determine radial force density $\boldsymbol{F}_r$. Due to typical low tangential and axial components of the flux density, the tangential and axial components are ignored for simplicity.

This is an observation of radial force for one fourth of the whole model. For both full and no-load conditions, Fig. 9 simulates and reports deviations in radial force with respect to radial distance.

For all topologies, spikes are generated in no-load and full-load conditions on both sides of the radial distance

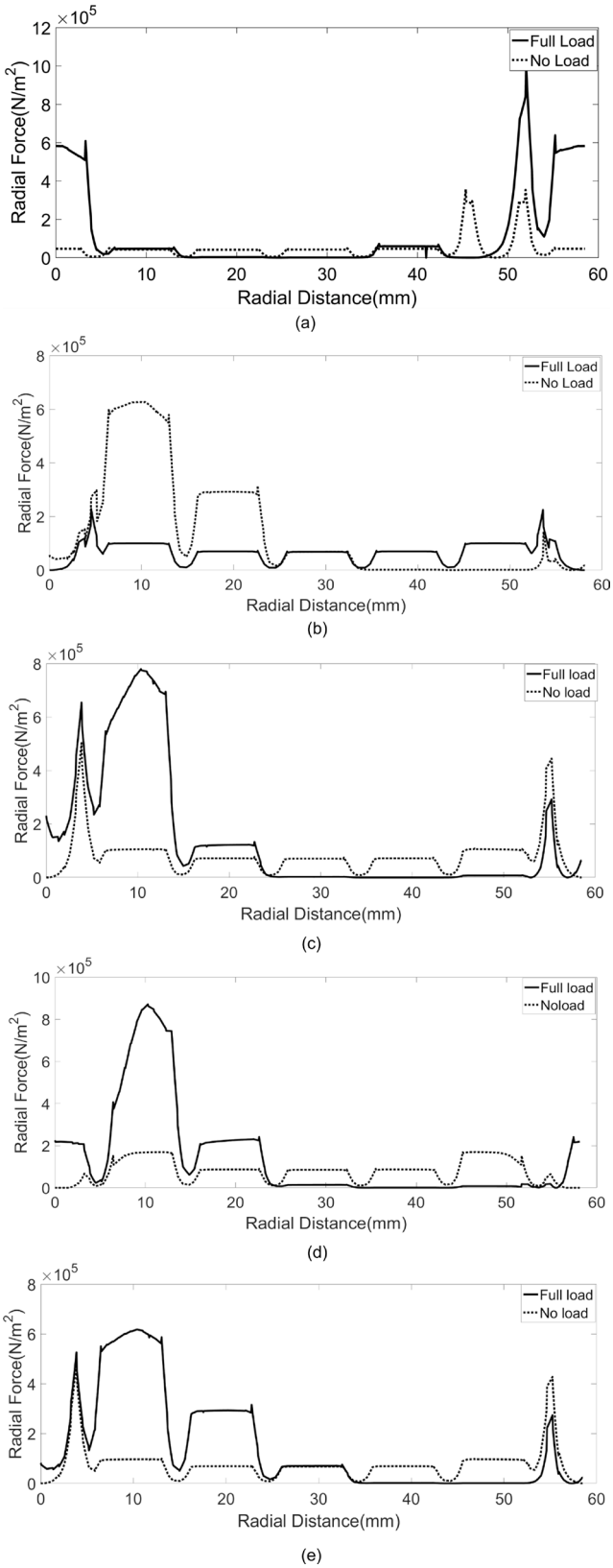

Fig. 9 Under full load and no-load condition radial force distribution at rated speed for (a) spoke shape; (b) saturable bridge; (c) V-shape; (d) radial shape; (e) segmented bridge

under study. There is no spike in the radial force under no load condition for any type of PMSM rotor topology except at the entry and exit points. Despite this, under full load condition, there is an increase in the non-uniformity of distribution of radial force in different parts of the rotor. Under full load condition, spoke shape rotors exhibit more spikiness in radial force at edging points of entry and exit section.

This topology does not have a continuous pulse in the middle section. Spikiness determines the roughness of a machine. The characteristics of a saturable and segmented bridge rotor under full load are similar, as shown in Fig. 9 (b) and Fig. 9 (e). The radial force on these two rotors is approximately equal under full load and the pulse patterns after each spike of the edging point are similar. The pulses are more non-uniform than those produced by a V-shaped or radial rotor. When it comes to a V-shaped motor, the magnitude of its radial force is much lower than when it comes to a cylindrical cylinder, as shown in Fig. 9 (c) and Fig. 9 (d). As a result of the radial force distribution, a motor's sensitivity to mechanical load is also determined. Motor performance is reduced as a result of this spikiness. When radial forces are not distributed evenly, the operation becomes imbalanced.

4.4 Characteristics of torque-speed

In all aspects of operation, PM-based machines are advantageous, including their high value of peak torque, their best dynamic response, and their low maintenance requirements [31]. Three different operating conditions of these motors are constant torque, fixed power, and decreasing power. As shown in Fig. 10, all five rotor topologies have torque-speed characteristics under rated conditions when termed as per unit (p.u.). Speed is varied between 500 and 4000 RPM. At rated speed 1500 rpm, each motor produces a different rated torque. For this analysis, per unit measurement is taken into account. A spoke shape has a torque of 2.18321 Nm under rated conditions. The per unit value of this motor is also higher than that of other motors. Other motors have already been mentioned with torque under rated conditions. IPM rotors with radial shapes have a wider speed range. Additionally, it has a better torque-speed performance throughout the entire speed range, compared to other types. With spoke types, constant torque is given only up to the rated speed before torque is reduced. Fig. 10 illustrates the nearly equal range of speed and similar torque characteristics for PMSM V-shape, u-shape, and segmented bridge rotors. When dealing with constant torque situations, spoke shape IPM motors have higher torque values. High speed causes saturation level to reach faster, so that constant speed ranges are higher than others.

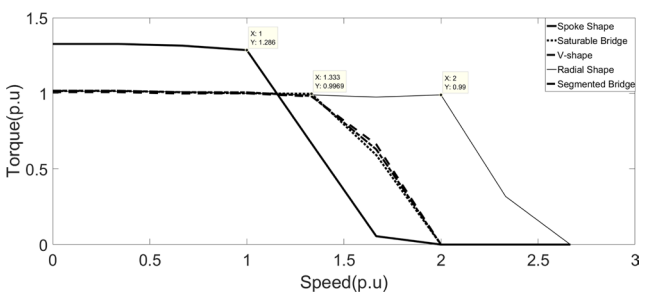

Fig. 10 Per unit value comparison of torque-speed characteristics of IPMSM under different rotor topology

As the rotor's magnetic field is suppressed, more d-axis current can be utilized in the armature current, and decreases the induced voltage. This widens the speed range of the rotor. As illustrated in Fig. 11, the induced phase voltage for all five topologies is plotted against the current excitation angle at 1.6 A and 1500 rpm under transient conditions. Also, IPM motors with radial shapes have the highest phase induced voltage, and those with spoke shapes have the lowest.

FEA is used to determine the torque characteristics of five types of PMSM rotors. A 2D transient analysis of maximum torque and current excitation angle is shown in Fig. 12. Compared with other topologies, torque for the

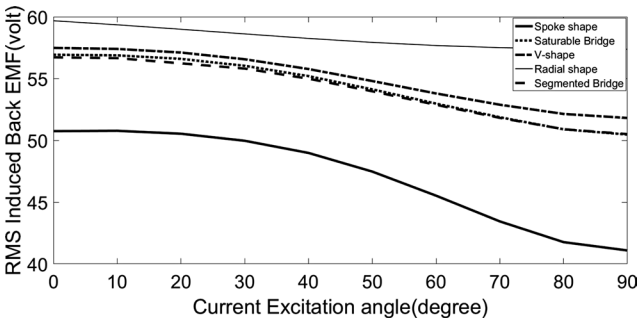

Fig. 11 Characteristics of induced voltage per phase of all five rotor topologies at base speed

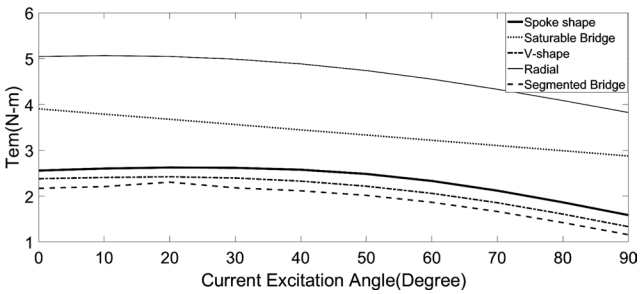

Fig. 12 Characteristics of electromagnetic torque (T_{em}) with respect to excitation angle for all five IPMSM rotor topologies

radial topology is more dependent on excitation angle. The characteristics of all motors decline as the angle increases. At zero current exciting angles, torque reaches its maximum value. During transient conditions, the voltage source leads by an angle $ø_r$. This prevents the torque from convergent to zero at 90 degrees.

For all rotor topologies, induced phase voltage characteristics are simulated under transient conditions and their comparison is presented in Fig. 13 (a). Induced phase voltages are equal for all rotor topologies except segmented bridges. At the rated speed of each motor, induced phase voltage is analyzed with FFT and presented in Fig. 13 (b). There is a greater difference between odd harmonics and even harmonics, and a fundamental component with the V-shape rotor topology is the smallest.

4.5 Mechanical stress analysis

Mechanical stress analysis is necessary to determine the distribution of mechanical stress over the rotor surface and its total deviation under transient conditions at high speed. Moreover, it gives a sense of the mechanical strength of the rotor parts. A motor speed of 3000 rpm is considered high in this paper. In addition to mechanical stress analysis, magnetostatic forces are also taken into account at various parts of a machine. An analysis is conducted using finite element analysis (FEA) to ensure the rotor integrity. For five different rotor topologies rotating at three thousand revolutions per minute at 20 °C, Fig. 14 shows the simulated von Mises stress distributions.

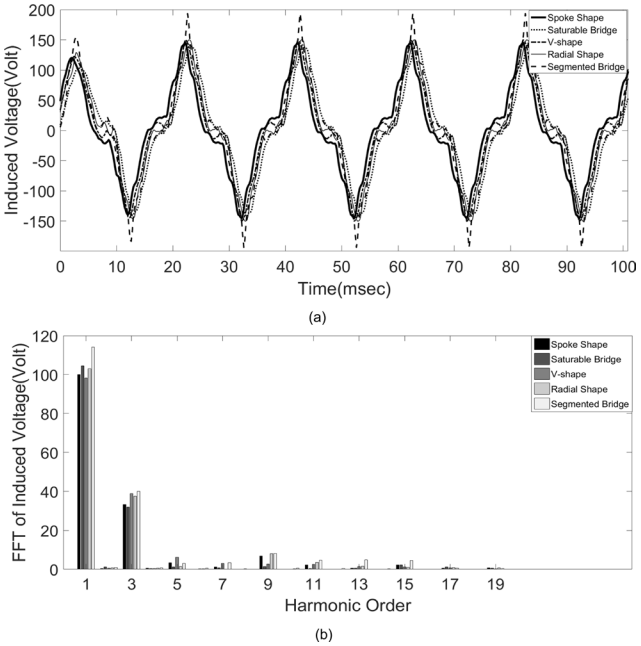

Fig. 13 Five topologies comparison by considering (a) Waveforms of induced phase voltage; and (b) FFT spectra of the induced phase voltage

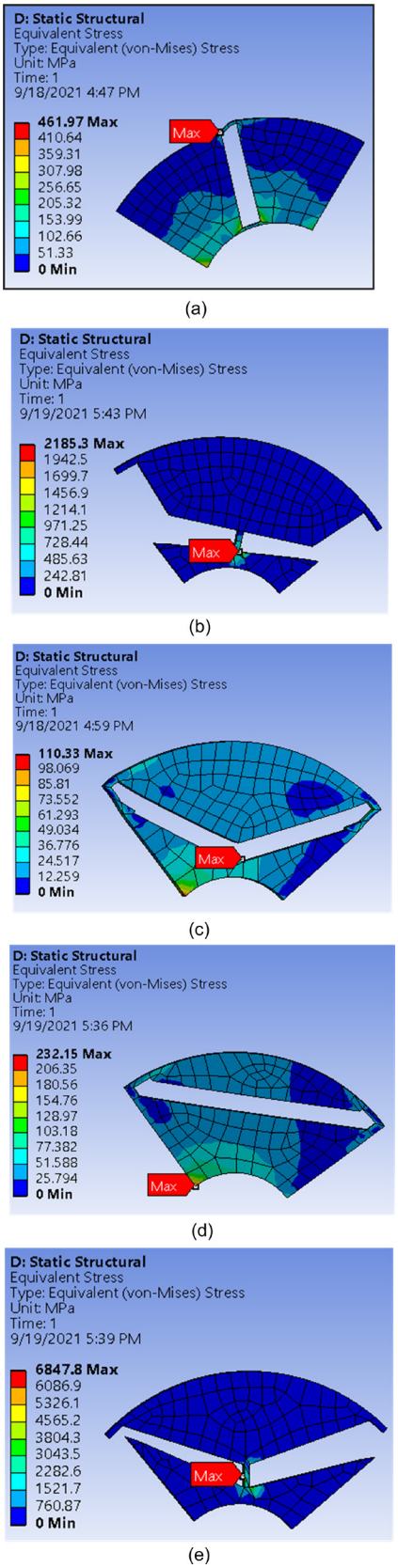

Fig. 14 von Mises stress distributions in the rotor under 3000 rpm, 22 °C of (a) spoke shape; (b) saturable bridge; (c) V-shape; (d) radial shape; (e) segmented bridge results from FEM simulation

When designing a motor, the flux bridges, which are buried beneath the permanent magnet on the rotor surface, are the first factor to consider. It is important to achieve sufficient magnetic saturation in the flux bridges before designing them in a machine. By doing so, its magnetic leakage flux will be minimized in the Rotor part. It is possible, however, to compromise the mechanical rigidity of a bridge by reducing the width too much. Additionally, the rotor surface does not have a uniform distribution of mechanical stress. In the considered topologies, 4 portions of the rotor are highly susceptible to high mechanical stress distribution. These areas are:

1. the upper bridges between permanent magnet pocket and rotor surface;
2. the lower section of rotor surface of placed PM;
3. the center bridge of PM in the rotor back iron; and
4. the inner edging surface part of rotor at the zone of shaft diameter.

As shown in Table 5, maximum stresses and their corresponding deformations are calculated under the conditions reported. In comparison with rest topologies, the V-shape has the lowest concentration of von Mises stress over the rotor surface. All five designs have one thing in common: mechanical stress isn't uniformly distributed across the surface of the rotor.

There is a variation based on specific regions. Fig. 14 (a) illustrates a high value of stress at the upper edge of the rotor in spoke shape. The rotor of a saturable bridge can be seen in Fig. 14 (b). Among the centralized magnets, the central bridge experienced the maximum von Misses stress distribution. When a V-shaped rotor is designed, maximum mechanical stress occurs at its center as in Fig. 14 (c). In comparison with other proposed rotor topologies, it is very low. A radial shape rotor shows similar mechanical stress reduction as the V-shaped rotor shown in Fig. 14 (d). However, the maximum stress produces at the inner edge of the rotor. According to Fig. 14 (e), the central bridge between two PMs is the point of maximum stress in the segmented bridge case. Among all the topologies studied, it has the highest stress. When centrifugal force causes displacement, deformation occurs. When strength limit of a certain material is exceeded by stress, deformation will be permanently fixed. Accordingly, all interrelated data are presented in Table 5 to find out the maximum possible deformation for each topology. The deformation of each topology is easily determined from stress distribution since deformation is linearly proportional to mechanical stress.

Table 5 Details of mechanical stress distribution and total displacement under high speed condition

Rotor of topology	von Mises stress	Deformation
Spoke shape	461.97 MPa	0.0377 mm
Saturable bridge	2185.30 MPa	1.7309 mm
V-shape	110.33 MPa	0.0095 mm
Radial shape	232.15 MPa	0.0211 mm
Segmented bridge	6847.80 MPa	4.1027 mm

5 Conclusion

This paper compares five IPMSMs based on their rotor topology designs and performance, including magnet thickness, magnetic flux density. The power ratings of all motors considered in the study are the same. Various modes of operation are considered when comparing IPM rotor performance. Comparisons are made based on torque, inductance along the *d*- and *q*-axes, output power, core loss, and efficiency. Furthermore, mechanical stress is observed for comparative purposes. In order to analyze the performance of all motors, 2D FEA is used. It is evident from the results that spoke-shaped PMSM rotors have high efficiency with 86.63%. Decaying of efficiency is not smooth when torque angle exceeds 90^0. Accordingly, for a wide range of torque angles, the V-shape rotor results better efficiency, with 85.5256% at maximum. Because of closest position of the magnet to the air gap, the radial shape IPMSM has the highest air gap flux density. Because the core loss in a spoke shape IPMSM is 18.70 W instead of 30 W, it has a lower core loss than other shapes. As far as flux density and magnetic force are concerned, V-shaped motors have a good surface. Rotor torque-speed characteristics are similar for saturable bridges, V-shapes, and segmented bridges. For wide speed range applications, radial motors are best.

References

[1] Iyer, K. L. V., Lai, C., Mukundan, S., Dhulipati, H., Mukherjee, K., Kar, N. C. "Investigation of Interior Permanent Magnet Motor With Dampers for Electric Vehicle Propulsion and Mitigation of Saliency Effect During Integrated Charging Operation", IEEE Transaction on Vehicular Technology, 68(2), pp. 1254–1265, 2019. https://doi.org/10.1109/TVT.2018.2865852

[2] Sayed, E., Abdalmagid, M., Pietrini, G., Sa'adeh, N.-M., Callegaro, A. D., Goldstein, C., Emadi, A. "A Review of Electric Machines in More/Hybrid/Turbo Electric Aircraft", IEEE Transactions on Transportation Electrification, 7(4), pp. 2976–3005, 2021. https://doi.org/10.1109/TTE.2021.3089605

[3] Bianchi, N., Bolognani, S., Carraro, E., Castiello, M., Fornasiero, E. "Electric Vehicle Traction Based on Synchronous Reluctance Motors", IEEE Transaction on Industrial Applications, 52(6), pp. 4762–4769, 2016.
https://doi.org/10.1109/TIA.2016.2599850

[4] Jo, I.-H., Lee, J., Lee, H.-W., Lee, J.-B., Lim, J.-H., Kim, S.-H., Park, C.-B. "A Topology Study for the Application of Magnetic Geared Motor as Traction for Urban Railway Vehicle", Journal of Electrical Engineering & Technology, 18(6), pp. 4473–4479, 2023.
https://doi.org/10.1007/s42835-023-01397-z

[5] Hwang, M.-H., Han, J.-H., Kim, D.-H., Cha, H.-R. "Design and Analysis of Rotor Shapes for IPM Motors in EV Power Traction Platforms", Energies, 11(10), 2601, 2018.
https://doi.org/10.3390/en11102601

[6] Mishra, A., Agarwal, P., Srivastava, S. P. "A comprehensive analysis and implementation of vector control of permanent magnet synchronous motor", International journal of Power Energy Conversations, 5(1), pp.1–23, 2014.
https://doi.org/10.1504/IJPEC.2014.059982

[7] Ge, B., Liu, M., Dong, J., Liu, W. "Torque Production Limit of Surface Permanent Magnet Synchronous Machines and Their Electromagnetic Scalability", IEEE Transactions on Industrial Applications, 57(5), pp. 4353–4362, 2021.
https://doi.org/10.1109/TIA.2021.3084552

[8] Dong, J., Huang, Y., Jin, L., Lin, H. "Comparative Study of Surface-Mounted and Interior Permanent-Magnet Motors for High-Speed Applications", IEEE Transaction on Applied Superconductivity, 26(4), 5200304, 2016.
https://doi.org/10.1109/TASC.2016.2514342

[9] Jia, L., Lin, K., Lin, M., Le, W., Wang, S. "Comparative Analysis of Dual-Rotor Modular Stator Axial-Flux Permanent Magnet Machines with Different Rotor Topologies", IEEE Transaction on Applied Superconductivity, 31(8), 5204405, 2021.
https://doi.org/10.1109/TASC.2021.3091124

[10] Agamloh, E., von Jouanne, A., Yokochi, A. "An Overview of Electric Machine Trends in Modern Electric Vehicles", Machines, 8(2), 20, 2020.
https://doi.org/10.3390/machines8020020

[11] Ou, J., Liu, Y., Doppelbauer, M. "Comparison Study of a Surface-Mounted PM Rotor and an Interior PM Rotor Made from Amorphous Metal of High-Speed Motors", IEEE Transaction on Industrial Electronics, 68(10), pp. 9148–9159, 2021.
https://doi.org/10.1109/TIE.2020.3026305

[12] Katona, M., Bányai, D. G., Németh, Z., Kuczmann, M., Orosz, T. "Remanufacturing a Synchronous Reluctance Machine with Aluminum Winding: An Open Benchmark Problem for FEM Analysis", Electronics, 13(4), 727, 2024.
https://doi.org/10.3390/electronics13040727

[13] Song, J.-Y., Lee, J. H., Kim, Y.-J.,Jung, S.-Y. "Computational Method of Effective Remanence Flux Density to Consider PM Overhang Effect for Spoke-Type PM Motor with 2-D Analysis Using Magnetic Energy", IEEE Transaction on Magnetics, 52(3), 8200304, 2016.
https://doi.org/10.1109/TMAG.2015.2475266

[14] Al-Jubori, W. K. S., Ahmed, Y. A. "Study and analysis the effect of variable applied voltage on SCIM performances based on FEA", International Journal of Power Electronics Drive System (IJPEDS), 11(3), pp. 1230–1240, 2020.
https://doi.org/10.11591/ijpeds.v11.i3.pp1230-1240

[15] Qu, G., Fan,Y., Wu, Z. "Design and Analysis of a New Hybrid-Excited Permanent Magnet Machine With Unequal Teeth", IEEE Transaction on Magnetics, 55(7), 8105805, 2019.
https://doi.org/10.1109/TMAG.2019.2907094

[16] Yoo, C.-H. "A New Multi-Modal Optimization Approach and Its Application to the Design of Electric Machines", IEEE Transaction on Magnetics, 54(3), 8202004, 2018.
https://doi.org/10.1109/TMAG.2017.2749506

[17] Khan, B., Khan, F., Ullah, W., Umair, M., Hussain, S. "Slot Filling Factor Calculation and Electromagnetic Performance of Single Phase Electrically Excited Flux Switching Motors", ACES Journal, 35(8), pp. 922–928, 2020.
https://doi.org/10.47037/2020.ACES.J.350811

[18] Wu, Z., Zuo, S., Hu, S., Hu, X. "Analytical modelling of air-gap magnetic field of interior permanent magnet synchronous motors", IET Electric Power Application, 14(11), pp. 2101–2110, 2020.
https://doi.org/10.1049/iet-epa.2019.0948

[19] Purwanto, W., Risfendra, Fernandez, D., Putra, D. S., Sugiarto, T. "Design and comparison of five topologies rotor permanent magnet synchronous motor for high-speed spindle applications", International Journal of GEOMATE, 13(40), pp. 148–154, 2017.
https://doi.org/10.21660/2017.40.02765

[20] Zhai, L., Hu, G., Song, C., Lv, M., Zhang, M. "Comparison of Two Filter Design Methods for Conducted EMI Suppression of PMSM Drive System for Electric Vehicle", IEEE Transaction on Vehicular Technology, 70(7), pp. 6472–6484, 2021.
https://doi.org/10.1109/TVT.2021.3080924

[21] Kovacik, M., Rafajdus, P., Kocan, S. "Comparison of Various PMSM Rotor Topologies for High-speed Drives in Automotive Applications", Transportation Research Procedia, 55, pp. 995–1002, 2021.
https://doi.org/10.1016/j.trpro.2021.07.070

[22] Yang, Y., Castano, S. M., Yang, R., Kasprzak, M., Bilgin, B., Sathyan, A., Dadkhah, H., Emadi, A. "Design and Comparison of Interior Permanent Magnet Motor Topologies for Traction Applications", IEEE Transactions on Transportation Electrification, 3(1), pp. 86–97, 2017.
https://doi.org/10.1109/TTE.2016.2614972

[23] Katona, M., Kuczmann, M., Orosz, T. "Accuracy of the robust design analysis for the flux barrier modelling of an interior permanent magnet synchronous motor", Journal of Computational and Applied Mathematics, 429, 115228, 2023.
https://doi.org/10.1016/j.cam.2023.115228

[24] Hemsen, J., Negri, T., Trost, C., Eckstein, L. "Comparison of Permanent Magnet Rotor Designs for Different Vehicle Classes and Driving Scenarios: A Simulation Study", SAE International Journal of Electrified Vehicles, 10(2), pp. 207–226, 2021.
https://doi.org/10.4271/14-10-02-0016

[25] Wang, Z., Yao, B., Guo, L., Jin, X., Li, X., Wang, H. "Initial Rotor Position Detection for Permanent Magnet Synchronous Motor Based on High-Frequency Voltage Injection without Filter", World Electric Vehicle Journal, 11(4), 71, 2020.
https://doi.org/10.3390/wevj11040071

[26] Pechlivanidou, M. C., Chasiotis, I. D., Karnavas, Y. L. "A comparative study on 2D and 3D magnetic field analysis of permanent magnet synchronous motor using FEM simulations", Journal of Electromagnetics Waves Applications, 33(17), pp. 2215–2241, 2019.
https://doi.org/10.1080/09205071.2019.1674190

[27] Torrent, M., Perat, J. I., Jiménez, J. A. "Permanent Magnet Synchronous Motor with Different Rotor Structures for Traction Motor in High Speed Trains", Energies, 1549, 2018.
https://doi.org/10.3390/en11061549

[28] Kim, H.-J., Moon, J.-W. "Improved rotor structures for increasing flux per pole of permanent magnet synchronous motor", IET Electric Power Applications, 12(3), pp. 415–422, 2018.
https://doi.org/10.1049/iet-epa.2017.0432

[29] Zhang, W., Zou, X., Sun, J. "Influence of Electromagnetic Characteristics of Shaft Material on the Performance of Induction Motor", International Journal of Emerging Electric Power System, 20(5), 20190080, 2019.
https://doi.org/10.1515/ijeeps-2019-0080

[30] Kang, Y. G., Reigosa, D., Sarlioglu, B., Lorenz, R. D. "D- And Q-Axis Inductance Estimation and Self-Sensing Condition Monitoring Using 45° Angle High-Frequency Injection", IEEE Transaction on Industrial Applications, 57(1), pp. 506–515, 2021.
https://doi.org/10.1109/TIA.2020.3029993

[31] Kül, S., Bilgin, O., Mutluer, M. "Application of Finite Element Method to Determine the Performances of the Line Start Permanent Magnet Synchronous Motor", Procedia - Social and Behavioural Sciences, 195, pp. 2586–2591, 2015.
https://doi.org/10.1016/j.sbspro.2015.06.458